

The net GHG balance and budget of the permafrost region (2000-2020) from ecosystem flux upscaling

Justine Ramage¹, McKenzie Kuhn¹, Anna-Maria Virkkala¹, Ana Bastos¹, Josep G. Canadell¹, Philippe Ciais¹, Benjamin Poulter¹, Jennifer Watts¹, Carolina Voigt¹, Maija E. Marushchak¹, Christina Biasi¹, Efrèn López-Blanco¹, Susan M. Natali¹, David Olefeldt¹, Stefano Potter¹, Brendan M. Rogers¹, Edward A.G. Schuur¹, Claire Treat¹, Merritt R. Turetsky¹, and Gustaf Hugelius¹

¹Affiliation not available

September 11, 2023

Abstract

The northern permafrost region has been projected to shift from a net sink to a net source of carbon under global warming. However, estimates of the contemporary net greenhouse gas (GHG) balance and budgets of the permafrost region remain highly uncertain. Here we construct the first comprehensive bottom-up budgets of CO₂, CH₄, and N₂O across the terrestrial permafrost region using databases of more than 1000 *in-situ* flux measurements and a land cover-based ecosystem flux upscaling approach for the period 2000-2020. Estimates indicate that the permafrost region emitted a mean annual flux of 0.36 (-620, 652) Tg CO₂-C y⁻¹, 38 (21, 53) Tg CH₄-C y⁻¹, and 0.62 (0.03, 1.2) Tg N₂O-N y⁻¹ to the atmosphere throughout the period. While the region was a net source of CH₄ and N₂O, the CO₂ budget was near neutral with large uncertainties. Terrestrial ecosystems remained a CO₂ sink, but emissions from fire disturbances and inland waters largely offset the sink in vegetated ecosystems. Including lateral fluxes, the permafrost region was a net source of C and N, releasing 136 (-517, 821) Tg C y⁻¹ and 3.2 (1.9, 4.8) Tg N y⁻¹. Large uncertainty ranges in these estimates point to a need for further expansion of monitoring networks, continued data synthesis efforts, and better integration of field observations, remote sensing data, and ecosystem models to constrain the contemporary net GHG budgets of the permafrost region and track their future trajectory.

1 Introduction

The northern permafrost region covers up to 21 million km² of land in the Northern Hemisphere of which ca. 70% (14 million km²) is entirely underlain by permafrost (Obu et al. 2021) – ground that is at or below 0°C for at least two consecutive years. Unprecedented and amplified increases in air temperature in the Arctic (Rantanen et al. 2022) have strong impacts on the permafrost ground temperatures and extent (Biskaborn et al. 2019; Li et al. 2022), with future climate projections indicating a potential loss of permafrost extent of 4.0 (-1.1+1.0, 1σ confidence interval) million km² for each °C of global temperature change (Chadburn et al. 2017). Consequences are already visible, as ground temperatures near the depth of zero annual amplitude in the continuous permafrost zone increased by 0.39 +/- 0.15 degC between 2007 and 2016, reducing the permafrost extent by 7% between 1969 and 2018 (Biskaborn et al. 2019; Li et al. 2022). Changes in ground temperature exposes substantial quantities of organic carbon (C), resulting in C degradation and atmospheric release of greenhouse gases (GHGs) such as carbon dioxide (CO₂), methane (CH₄), and nitrous

oxide (N_2O) from permafrost into the atmosphere (Schuur et al. 2009, Schuur et al. 2015; Treat et al. 2018; Natali et al. 2019; Chen et al. 2021, Voigt et al. 2020).

This release of GHGs to the atmosphere could have a strong impact on the global carbon cycle as the upper three metres of permafrost region soils are estimated to store 1000 ± 200 Pg (1 Pg = 1000 Tg) of soil organic carbon (Hugelius et al. 2014, Mishra et al. 2021) and 55 Pg of soil nitrogen (N) (Palmtag et al. 2022). Deeper deposits store an additional 400-1000 Pg C, making the permafrost region the largest terrestrial carbon and nitrogen pool on Earth (Schuur et al. 2022, Strauss et al. 2021). These soil C and N have been accumulating over thousands of years due to limited microbial decomposition at low temperatures and water-logged conditions, leading to long-term accumulation of organic matter and incorporation into permafrost (Tarnocai et al. 2009). Upon thaw – that can occur gradually or abruptly – permafrost landscapes are changing, impacting their hydrology and biogeochemical cycling (e.g. Christensen et al. 2020), creating a potentially significant feedback to the global climate (Schuur et al. 2008; Schuur et al. 2015; Schuur et al. 2022). The release of GHGs from permafrost has the potential to accelerate global climate warming, known as the “permafrost carbon feedback” (Schuur et al. 2015, Burke et al. 2017, Burke et al. 2022). While longer growing seasons, increased CO_2 concentrations, and additional nutrient release from thawing permafrost may lead to increased vegetation productivity and partly offset the release of permafrost GHGs (Koven et al., 2015; McGuire et al., 2018; Liu et al., 2022; Schuur and Mack, 2018; Lopez-Blanco et al., 2022), other processes such as disturbances cause rapid shifts to landscape structure (Schuur et al., 2008; Schuur et al., 2011) and might accelerate the release of GHGs into the atmosphere.

Although presumably crucial for the global carbon cycle, the role of the northern permafrost region in the global carbon budget is unknown. Existing estimates of terrestrial GHG exchange from land cover-based or machine learning-based ecosystem vertical flux upscaling identify the northern permafrost terrestrial ecosystem as a net sink of CO_2 (-181 Tg $\text{CO}_2\text{-C y}^{-1}$, Virkkala et al. 2021) and a net source of N_2O (0.14 Tg $\text{N}_2\text{O-N y}^{-1}$, Voigt et al. 2020), although large uncertainties remain. The northern permafrost region GHG budgets remain poorly constrained as our understanding of the GHG balance of this region has been hampered by low data availability (both temporal and spatial) and a heterogeneous landscape that is complex to map accurately. Watts et al (2023) show that in northern high latitude, the Net Ecosystem Carbon Budget (NECB) is reduced by ca. 7% when inland waters (e.g. lakes, ponds, streams, and rivers) – known to be significant emitters of CO_2 and CH_4 (Cole et al. 2007; Stanley et al. 2016; Thornton et al. 2016; Wik et al. 2016; Stackpoole et al. 2017; Serikova et al. 2018) – are included, and by ca. 30% when emissions from inland waters and fires are considered. However, no study has yet included inland waters and disturbances to constrain the GHG budget of the permafrost region and provide an overall net GHG balance.

Here we fill this gaps and present comprehensive budgets of GHGs (CO_2 , CH_4 , and N_2O), by key permafrost land cover types over the period 2000-2020 across the northern permafrost region using a single flux upscaling approach for all three GHGs. We include most relevant ecosystem components that include terrestrial ecosystems, inland waters, geological fluxes, lateral fluxes, and fire fluxes.

This permafrost regional budget is part of the REgional Carbon Cycle Assessment and Processes-2 (RECCAP2) project of the Global Carbon Project that aims to collect and integrate regional GHGs budgets for 12 land regions and 5 ocean basins covering all global lands and oceans (Ciais et al. 2022; <https://www.globalcarbonproject.org/reccap/>). Comparisons of GHG budgets using this upscaling flux approach and budgets based on atmospheric inversion models and terrestrial process-based models are discussed in Hugelius et al. (*in prep*).

2 Materials and Methods

2.1 Study area

The spatial extent of permafrost defined in this study includes areas within the northern permafrost region as defined in Obu et al. (2021) and restricted to the Boreal Arctic Wetlands and Lakes Dataset area that had the key land cover classes for our upscaling (BAWLD, Olefeldt et al. 2021a,b) (Fig. 1). As a consequence, the BAWLD-RECCAP2 permafrost region does not include large areas underlain by permafrost in Central Asia and the Tibetan plateau. The BAWLD-RECCAP2 permafrost region considered in this study is 18.5 million km². All flux estimates were scaled to the BAWLD-RECCAP2 permafrost region (hereafter permafrost region). The study area overlaps several other RECCAP2 regions (Ciais et al. 2022), and no specific effort to harmonise the budgets presented here with the RECCAP2 budgets of those regions is made in this paper.

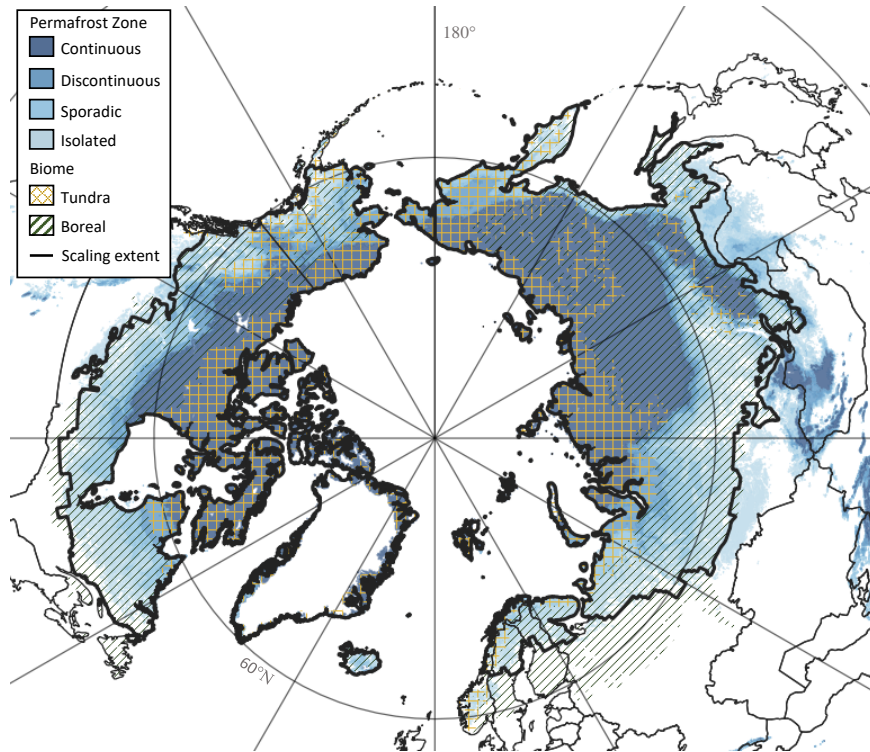


Figure 1. Map of northern permafrost extent (data from Obu et al. 2021) overlain with the spatial extent of the permafrost domain included (BAWLD-RECCAP2 regions). The spatial extent of the permafrost region defined in this study as an overlap of permafrost extent and the Boreal Arctic Wetlands and Lakes Dataset (BAWLD, Olefeldt et al. 2021a,b). Figure A1 in the supplement shows the additional areas that recorded mean annual air temperature (MAAT) below 0°C between 1990 and 2000 (full extent of ISIMIP3 permafrost model intercomparison), but which were excluded from this budget estimate because they are outside the BAWLD extent.

2.2 GHG budgets from ecosystem flux upscaling

Data-driven ecosystem flux upscaling of GHG budgets for a reference time period of 2000-2020 was calculated by summing up flux budgets from terrestrial ecosystems, inland waters, lateral fluxes, fire emissions, and geological fluxes. To calculate the total net regional GHG flux (F_x), we used the following equation:

$$F_x = \sum_{j=1}^{j=n} A_j \times F_{jx}$$

where F_x is annual permafrost region gas flux for the GHG species of interest x , A_j is the area of each land cover class j (Fig. 2, Table A1), and F_{jx} is the land cover average GHG flux density for species x (Table A1).

We used existing synthesis databases and upscaled gridded data products published in the past five years to estimate annual and growing season mean fluxes per land cover type. All budget numbers are presented as the weight of C and N (i.e. CO₂-C, CH₄-C and N₂O-N yr⁻¹), not as the weight of GHG molecules. Budgets are reported as mean fluxes with 95% confidence intervals (CI) in Tg C or N.

2.3 GHG fluxes from terrestrial land cover types

The land cover classification used for the analysis was adapted from the Boreal-Arctic Wetland and Lake Dataset (BAWLD) land cover (Olefeldt et al. 2021a,b). The BAWLD land cover classes are distinguished based on moisture regime, nutrient/pH regime, organic-soil depth, hydrodynamics, and the presence or absence of permafrost (Olefeldt et al. 2021a). To match the observational GHG flux datasets, we simplified the nine terrestrial land cover classes in BAWLD into five: Boreal Forests; Non-permafrost Wetlands; Dry Tundra; Tundra Wetlands; and Permafrost Bogs (Fig. 2). Classes were defined as:

- *Non-permafrost Wetlands* include permafrost free bogs, fens, and marshes with no near-surface permafrost (see Canadian Wetland Classification system).
- *Boreal Forests* are forested ecosystems with non-wetland soils. Coniferous trees are dominant, but the class also includes deciduous trees in warmer climates and/or certain landscape positions. Boreal Forests ecosystem may have permafrost or be permafrost free.
- *Permafrost Bogs* are ecosystems with near surface permafrost and thick surface peat layers (>40 cm). This includes palsas, peat plateaus, and the elevated portions of high- and low-centre polygonal permafrost bogs. They typically have ombrotrophic conditions that cause nutrient-poor conditions. The vegetation is dominated by lichens, Sphagnum mosses, woody shrubs, and sometimes sparse coniferous forest.
- *Dry Tundra* include treeless ecosystems (both lowland arctic and alpine tundra) dominated by graminoid or shrub vegetation. Dry Tundra ecosystems generally have near-surface permafrost. Dry Tundra is differentiated from Permafrost Bogs by their thinner organic soil (<40 cm), and from Tundra Wetlands by their drained soils (average water table position >5 cm below soil surface).
- *Tundra Wetlands* are treeless ecosystems with near surface permafrost and saturated to inundated conditions for large parts of the year. Tundra Wetlands can both be mineral (<40 cm peat) or have peat (>40 cm peat). They are distinguished from Dry Tundra and Permafrost Bogs by being wetter and having more dynamic hydrology. Tundra Wetlands includes areas that can be classified as tundra fen wetlands in the Canadian Wetland Classification System.

This choice of land cover classes was done after assessing the type of sites in three flux databases of CO₂, CH₄, and N₂O used for the upscaling (see description below), ensuring that there was sufficient data for each class and that the merging was the most parsimonious grouping that allowed us to estimate each GHG balance

for each class. Due to a lack of flux data, rocklands and glaciers were not included in the classification. The area of each land cover class (A_j) in km^2 across the permafrost region is shown in Figure 2 and detailed in Table A1.

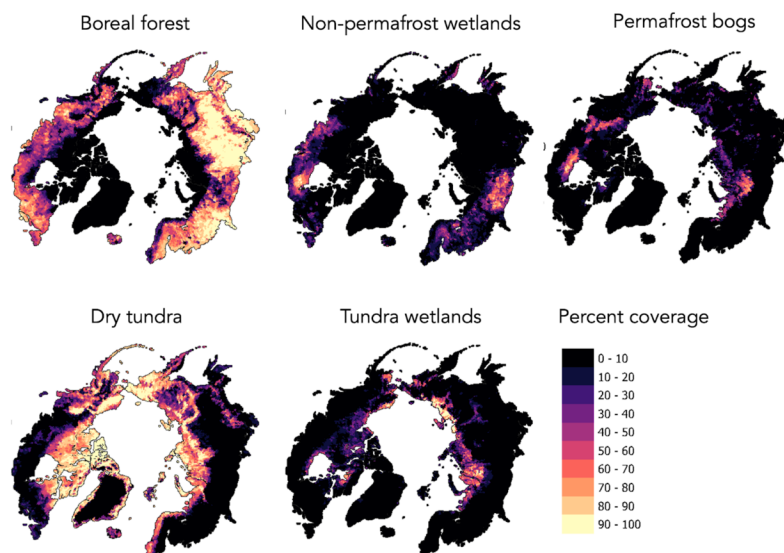


Figure 2 . Circumpolar percentage coverage of the five adapted BAWLD terrestrial land cover types (Boreal Forests, Non-permafrost Wetlands, Permafrost Bogs, Dry Tundra, and Tundra Wetlands) used for ecosystem-based upscaling of GHG flux budgets in this study. Note that these maps show the distributions across the full BAWLD domain as presented by Olefeldt et al (2021), not the more limited extent of the RECCAP2 permafrost BAWLD domain used in this study.

The land cover mean GHG flux ($F_{j,x}$) were obtained for each of the five terrestrial land cover classes after homogenising and analysing three comprehensive GHG flux datasets: Virkkala et al. (2022) for CO_2 fluxes; Kuhn et al. (2021a) for CH_4 fluxes; and Voigt et al. (2020) for N_2O fluxes. Additional data was extracted from literature for Boreal Forest N_2O fluxes (Schiller and Hastie, 1996; Simpson et al., 1997; Kim and Tanaka, 2003; Morishita et al. 2007; Matson et al. 2009; Ullah et al. 2009; Köster et al. 2018a), since the N_2O flux dataset from Voigt et al. (2020) does not cover Boreal Forest ecosystems. These datasets comprise roughly 1000 *in-situ* growing-season and annual observations (including multiple observations from some sites) of terrestrial fluxes obtained from more than 200 sites using chamber (for CH_4 , N_2O , and CO_2), diffusion (for CH_4 and CO_2), and eddy covariance (for CO_2 and CH_4) methods. The growing season length was defined as June to August (90 days) for the tundra and permafrost bogs sites, and May to September (150 days) for the Boreal Forests and Non-Permafrost Wetlands. The CO_2 dataset comprises year-round measurements of net ecosystem exchange (NEE), which we used to calculate growing season and annual NEE. Average fluxes were calculated based on 93 sites and 403 observations for growing season NEE and 54 sites and 222 observations for annual NEE. The CH_4 and N_2O datasets provide growing-season measurements based on 98 sites and 458 observations of CH_4 exchange and 47 sites and 91 observations of N_2O exchange. For sites with incomplete growing season measurements, we multiplied average daily fluxes to the length of the growing season. Annual CH_4 fluxes were estimated assuming that growing season emissions accounted for 64% of annual emissions (Treat et al. 2018), except for boreal forests where we assumed growing season emissions accounted for 100% of annual emissions as the sites averaged net CH_4 growing season uptake and available data for winter season fractions only covers CH_4 -emitting ecosystems (Treat et al. 2018). Our Boreal Forest annual estimate should therefore be considered conservative. Annual N_2O fluxes were estimated assuming

that growing season emissions accounted for 50% of annual emissions as reported in Voigt et al. (2020). For all three GHGs, only sites with no record of large-scale upland hillslope abrupt thaw disturbance in the metadata were included in the flux estimates to avoid double-counting emissions from upland hillslope abrupt thaw (see methodology for disturbances). However, although scarce, we included other disturbed sites in our CO₂ estimates to account for ecosystem CO₂ losses following disturbances and their different successional stages (e.g., 4 sites reporting thermokarst; Virkkala et al. 2022). Sites from the above-mentioned GHG flux datasets were classified into one of the five terrestrial land cover classes using the metadata provided in each of the datasets. More details on how ecosystem flux upscaling was performed can be found in the supporting information.

While the focus of this study is the period 2000-2020, we include all *in-situ* measurements obtained between 1991 and 2020 in order to overcome the limited amount of flux measurements in some of the ecosystems and therefore ensure adequate spatial representation of ecosystem fluxes. A separate analysis of decadal CO₂ fluxes from 1991 to 2020 revealed no differences, suggesting that the extension of time series to 1991 does not impact our findings (Table A2).

2.4 GHG fluxes from inland waters

Similarly to the method used to calculate GHG emissions from terrestrial land cover types, GHG fluxes from inland waters were calculated by upscaling mean GHG fluxes from lakes and rivers (see below) using the estimated surface area of these aquatic classes from the BAWLD classification (Olefeldt et al. 2021), adjusted to the study region (see supplementary Table A1 for estimated aerial extent of inland waters).

GHG budgets for rivers

Atmospheric riverine GHG fluxes were calculated in different ways for each GHG, depending on available source data, and when possible scaled across the region using riverine area from the permafrost region (0.12 x 10⁶ km²), reported in BAWLD.

Estimates of river and stream CO₂ flux were calculated from gridded monthly flux data estimated by Liu et al. (2021; <https://doi.org/10.5061/dryad.d7wm37pz9>; Dryad) from river water dissolved CO₂ pressure and gas transfer velocity. We combined the monthly fluxes from the start of May to the end of October, assuming that this corresponds to the ice-free season (when water-to-air gas transfer can occur). This time extent (184 days) is nine days longer than the duration Liu et al. (2022) cite as the mean ice-free period for Arctic lakes (175 days). This data is delivered as unprojected global grids with a 0.0083 degree resolution (which is ca 1*0.2 km pixels in the high Arctic). The global grids were clipped to the extent of BAWLD and then reprojected to an equal area grid at 100*100 m resolution. Calculations from this data yields a total stream and river area of 0.069*10⁶ km², and a total flux of 94 Tg CO₂-C yr⁻¹. Assuming the mean river flux (1,370 g C m⁻² yr⁻¹) can be scaled also to smaller streams and rivers, we applied the area of streams and rivers in BAWLD (0.12*10⁶ km²). Because spatially explicit estimates of uncertainty are not available, we report a coefficient of variation proportional to the global uncertainty reported by Liu et al. (2022). Riverine CH₄ emissions were determined using the mean CH₄ diffusive flux reported in the MethDB (Stanley et al. 2016). Stanley et al. (2016) found that diffusive CH₄ emissions did not statistically differ across latitudes and scaled global river CH₄ emissions using one mean value. Given the limited number of reported CH₄ fluxes for rivers in the Arctic (e.g. Zolkos et al. 2020), we used the same approach as Stanley et al. (2016) and applied a global mean diffusive flux of 135 mg CH₄m⁻² d⁻¹ to the river area. Because there are few studies that measure CH₄ emissions upon ice-out, we applied for CH₄ a conservative estimate that 17% of annual fluxes occur during the ice-free period (Denfield et al. 2018; consistent with the approach by Liu et al. 2022). Ebullition was not included for river CH₄ emission estimates due to few available measurements

in the literature for this region (Stanley et al. 2016). Estimates of river N₂O flux were derived from gridded annual N₂O flux estimated by a mechanistic mass balance model developed globally for inland waters by Maavara et al. (2019). These data was reprojected from an original 0.5 degree unprojected grid to an equal area grid at 1 km resolution and clipped to the BAWLD extent. As the original lake and river surface area was not known, no correction of inland water surface area was made. Uncertainties for river GHG budgets were determined using the standard error and coefficient of variance reported by Liu et al. (2022), Stanley et al. (2016) and Maavara et al. (2019), respectively, for CO₂, CH₄, and N₂O.

GHG budgets for lakes

CH₄ fluxes (diffusion and ebullition) were extracted from the BAWLD-CH₄ aquatic ecosystem dataset and classified based on classes (yedoma lakes, peatland ponds, and glacial/post-glacial organic poor lakes and ponds) and sizes, from large (> 10 km²) to midsize (0.1 to 10 km²) to small lakes (< 0.1 km²) (Kuhn et al. 2021a; total area = 1.255 10⁶ km²; Table A3). Notably, no minimum size for lakes was considered in the BAWLD dataset, as the dataset gives an estimate of the overall area covered by lakes in each size-class (Olefeldt et al. 2021). Conceptually, any area which is likely to be inundated >50% of the growing season period (long term average) is considered part of the lake land cover classes. Ice-free days were determined based on averages of reported ice-free days for each lake type and this information was used to determine ice-free season fluxes (supplementary Table A1). In addition to ice-free emissions, spring ice-out emissions (i.e. winter contribution) were considered to be 23% of the annual total (Wik et al. 2016).

Estimated lake CO₂ fluxes were compiled from multiple available sources based on a literature search made in May 2022 (Humborg et al. 2010; Rocher-Ros et al. 2017; Karlsson et al. 2013; Sepulveda-Jauregui et al. 2015; Pelletier et al. 2014; Rasilo et al. 2014; Korteliane et al. 2006) and are summarised in Table A4). The studies report lake CO₂ fluxes as mean flux values for various binned lake surface areas. We took these averages and grouped them by the lake size classes included in BAWLD (<0.1, 0.1-10, >10 km²). We found no statistical differences in fluxes between the size groups and thus used one mean lake CO₂ flux to scale across the year and the region (315 ± 196 mg C m⁻² d⁻¹). We applied the same number of ice-free days used to scale lake CH₄ emissions (ice-free days reported in the literature for each lake class).

To estimate lake fluxes of N₂O, gridded global data of annual flux from Lauerwald et al. (2019) were used. This estimate is based on the nitrous oxide (N₂O) emission model developed by Maavara et al. (2019) and the HydroLAKES database and was reprojected from an original 0.5 degree unprojected grid to an equal area grid at 1 km resolution and clipped to the BAWLD extent. As the original lake and river surface area was not known, no correction of inland water surface area was made. Uncertainties for lake N₂O were determined using the coefficient of variance reported for regions north of 50 deg latitude in Lauerwald et al. (2019).

2.5 Disturbances - fires and abrupt thaw

Monthly GHG fire emissions were extracted for the study region from the Global Fire Emission Database version 4s (GFED; van der Werf et al. 2017). The GFED4s spans from 1997-2016 and estimates of burned areas are based on remote sensing data at a spatial resolution of 0.25 degrees (van der Werf et al. 2017). GHG emissions in the GFED4s are derived from the multiplication of burned area and fuel consumption per unit burned area, the latter being the product of modelled fuel loads per unit area and combustion completeness. For our purpose, we extracted mean annual GHG emissions from burned areas for the period 2000-2016 and assumed similar rates for the period 2016-2020.

Localised, but widespread, disturbances associated with abrupt thaw are thought to contribute significantly to GHG emissions from permafrost (Abbott and Jones, 2015, Yang et al. 2018, Walker et al. 2019, Turetsky

et al. 2020; Holloway et al. 2020, Marushchak et al. 2021, Runge et al. 2022). Abrupt thaw includes thawing processes that affect permafrost soils in periods of days to several years (Grosse et al. 2011), and is typically associated with thermokarst and thermoerosion processes that lead to the formation of hillslope erosional features (thaw slumps, thermo-erosion gullies and active layer detachments), thermokarst lakes, and thermokarst wetlands (i.e., collapse scar bogs and fens). We report abrupt thaw areas and derived annual CO₂ and CH₄ emissions using the inventory-based abrupt thaw model by Turetsky et al. (2020), in which atmospheric emissions are estimated for three generalised types of abrupt thaw terrains: mineral-rich lowlands, upland hillslopes, and organic-rich wetlands. In the abrupt thaw model, abrupt thaw areas are based on synthesised field observations and remote sensing measurements. GHG emissions from abrupt thaw were synthesised for each ecosystem state within each abrupt thaw type from the literature (ca. 20 published papers). The abrupt thaw model was initialised for a historical assessment period (1900-2000) to provide the model with a spin up and prevent the regional carbon fluxes starting at zero at the beginning of the dynamic measurement period. Thaw rates were generally in equilibrium with succession and recovery of surface permafrost during this initialization period. Changes in the area of each successional state were tracked over time by multiplying initial starting areas by transition rates. Estimates of abrupt thaw GHG emissions following the historical assessment period were done by increasing rates of abrupt thaw through time. This increase in thaw rate was prescribed to follow the average output of ‘permafrost-enabled’ land surface models, all of which were forced by atmospheric climate anomalies from the Community Climate System Model 4 (CCSM4) Earth system model under an RCP8.5 projection. For our purpose, we ran the abrupt thaw model for the period 2000-2020 and extracted cumulative CO₂ and CH₄ emissions from active and stabilised abrupt thaw features, and derived annual fluxes for each abrupt thaw terrain for the time period 2000-2020. We used the reported uncertainty ranges of +- 40% on the upland hillslope areas, +- 30% on the mineral-rich lowland areas, and +- 35% on the organic-rich wetland areas as in Turetsky et al. (2020). Additional details on the inventory model can be found in Turetsky et al. (2020). Since GHG datasets that we used for ecosystem upscaling partly account for abrupt thaw and to prevent double counting GHG fluxes, CO₂ and CH₄ fluxes from abrupt thaw were added as a sub-flux (not added to the total) of terrestrial and inland water land cover fluxes and their contribution to the total GHG budget is discussed. Due to the lack of in situ observations of abrupt thaw impacts on N₂O fluxes in the used datasets, no N₂O budget is presented for abrupt thaw.

2.6 Lateral fluxes and geological emissions

Lateral C and N fluxes from riverine transport and coastal erosion (i.e. DOC and DON losses from the permafrost region to the ocean) are taken from Terhaar et al. (2021), representative for all land north of 60deg N. They estimated riverine lateral fluxes for the six largest Arctic rivers (Mackenzie, Yukon, Kolyma, Lena, Ob, Yenisei) from the Arctic Great River Observatory (ArcticGRO) dataset and extrapolated to the entire Arctic catchment. Emissions from coastal erosion were calculated by multiplying spatially resolved estimates of coastal erosion rates by estimates of C content in coastal soils provided in Lantuit et al. (2012).

Estimates of geological emissions of CH₄ (from subsurface fossil hydrocarbon reservoirs) are taken from an upscaled circumpolar permafrost region estimate for gas seeps along permafrost boundaries and lake beds made by Walter Anthony et al. (2012). We note that there is some risk of double counting such fluxes, especially in sites where eddy covariance flux towers may have unknowingly been placed close to seeps of geological CH₄ emissions. No separate estimates of geological emission for CO₂ or N₂O are available for the permafrost region. For CO₂, the full global geological emissions are estimated to 0.16 Pg CO₂-C yr⁻¹ (Morner and Etiope 2002).

3 Results and Discussion

3.1 Net GHG exchange from terrestrial land cover types

Terrestrial ecosystems represented a decadal-scale sink for CO₂, and source for CH₄ and N₂O (Table 1, Fig. 3). The mean annual CO₂ flux was a net sink, but could not be distinguished from CO₂ neutral when the 95% confidence interval was considered (-339.6 (-835.5, 156.3) Tg CO₂-C y⁻¹). The broad uncertainty interval can be attributed both to the large natural variability in CO₂ fluxes across sites and to the heterogeneity of ecosystem types included in each of the land cover classes defined in the BAWLD classification. Boreal Forests and Non-permafrost Wetlands were CO₂sinks (-270.3 and -69.4 Tg CO₂-C y⁻¹, respectively) while Tundra Wetlands and Permafrost Bogs were close to neutral (-2.7 and -0.05 Tg CO₂-C y⁻¹, respectively). Dry Tundra was the only ecosystem type classified as an annual ecosystem CO₂ source (2.9 Tg CO₂-C y⁻¹), but the very broad uncertainty range (-147.6, 153.5 Tg CO₂-C y⁻¹) indicates low confidence in the sign of this flux. Terrestrial ecosystems were overall a net sink of CO₂ during the growing season (-1611 (-2148, -1074) Tg CO₂-C gs⁻¹), with the strongest sink in the boreal forest (-1034 (-1305, -763) Tg CO₂-C gs⁻¹) (Table 2).

Annual terrestrial CO₂ flux budgets have been reported for high-latitudes in recent papers using different upscaling approaches. While closely related due to overlap in flux data, a higher NEE uptake is reported by both Virkkala et al. (2021) and Watts et al. (2023) (-419 (95% CI of -559 to -189) Tg CO₂-C y⁻¹ and -601 (standard error of +- 1138) Tg CO₂-C y⁻¹, respectively). However the estimated NEE uptakes for the permafrost region solely are weaker, with an uptake of -181 (-305, 32) Tg CO₂-C y⁻¹ and -230 (+ 22) Tg CO₂-C y⁻¹, respectively). The difference between the later NEE uptakes and our results relates to the subset of data included in the analyses (exclusively eddy covariance tower fluxes in Watts et al. (2023)), the different years covered in the analyses (Virkkala et al. 2021: 1990-2015, Watts et al. 2023: 2003-2015), the different spatial extents, and the upscaling approach applied (Arctic Terrestrial Carbon Flux Model (TCFM-Arctic) in Watts et al. (2023), and statistical upscaling in Virkkala et al. (2021)). Both of these studies as well as the previous RECCAP synthesis (1990-2006, McGuire et al. 2012) report the tundra as a weak CO₂ sink (-13 (-81, 62); -16 (+84-270); and -16 (-42, 10) Tg CO₂-C y⁻¹, respectively) although they also show that annual tundra budgets cannot be distinguished from CO₂ neutral when taking into account the uncertainty range. Dry Tundra CO₂ budget was also identified as a source of 10 (-27, 47) Tg CO₂-C y⁻¹ in McGuire et al. (2012).

Our estimated annual net CH₄ source of 25.6 (14.7, 36.4) Tg CH₄-C y⁻¹ from terrestrial ecosystems (Table 1) was largely driven by emissions from Non-permafrost Wetlands (20.6 (14.3, 26.9) Tg CH₄-C y⁻¹). As in Treat et al. (2018), Non-permafrost Wetlands emitted more than Tundra Wetlands. Annual CH₄ flux estimates for Tundra Wetlands (3.3 (2.7, 3.9) Tg CH₄ y⁻¹) and Dry Tundra (2.1 (-0.4, 4.5) Tg CH₄-C y⁻¹) were in the lower range from the previous estimates provided in McGuire et al. (2012), in which the tundra was estimated to release 11 (0, 22) Tg CH₄-C y⁻¹ (between 1990 and 2006). Our growing season CH₄ budget was a source of 16 (8.6, 23.3) Tg CH₄-C gs⁻¹ (Table 2) with Non-permafrost Wetlands contributing 83%. All terrestrial ecosystems except Boreal Forests were net CH₄ emitters. Boreal Forests were a net sink of CH₄ (-1.1 (-2.3, 0.0) Tg CH₄-C gs⁻¹). Our CH₄ annual budget was lower than the ones estimated for the northern high latitude wetlands (>45degN) at 31, 32, and 35 Tg CH₄-C y⁻¹ (depending on wetland distribution maps) by Peltola et al. (2019) and 38 Tg CH₄-C y⁻¹ by Watts et al. (2023). However, our CH₄ growing season budget estimate was higher than the budget based on 93 observations presented in Treat et al. (2018) except for the Tundra Wetlands where they remain within the same range. Despite their large spatial coverage, Dry Tundra was a small source of CH₄ during the growing season (1.4 (-0.3, 2.9) Tg CH₄-C gs⁻¹), although the low end of the CI suggests that it could remain a sink. More measurements from these drier ecosystems are needed.

Our N₂O annual budget estimate of 0.55 (-0.03, 1.1) Tg N₂O-N y⁻¹ (Table 1) suggests that terrestrial ecosystems were a N₂O source, although the uncertainty range around N₂O fluxes extends from a small sink to a larger source. These high uncertainties partly relate to the limited number of observations of N₂O fluxes

(47 sites and 91 observations), which only includes growing-season observations. Our estimated annual N₂O budget is within the range of the one previously reported by Voigt et al. (2020)(0.14-1.27 Tg N₂O-N y⁻¹ median-mean-based estimate). In our study, Dry Tundra was the largest N₂O source (0.23 (0.04, 0.42) Tg N₂O-N y⁻¹). Boreal Forests were the second largest N₂O source (0.14 (-0.01, 0.30) Tg N₂O-N y⁻¹) due to their large area, although their fluxes per unit area were small (Table A5, 52.43 ug N₂O m⁻²d⁻¹). Although they occupy a small portion of the landscape (5%), Permafrost Bogs were the largest N₂O emitters per unit area (Table A5, 645.14 ug N₂O m⁻² d⁻¹) and their contribution to the regional budget was 18%. The estimate for Permafrost Bogs includes emissions from barren peat surfaces, where vascular plants are absent - surfaces previously identified as N₂O hot spots in the Arctic due to ideal conditions for N₂O production (Repo et al. 2019; Marushchak et al., 2011; Gil et al. 2017). A challenge remains regarding the mapping of Permafrost Bogs and barren ground and integration within land cover classifications. Therefore, we did not differentiate between vegetated and non-vegetated Permafrost Bog areas when upscaling. N₂O emissions from Tundra Wetlands were negligible (0.01 (0.00, 0.02) Tg N₂O-N y⁻¹), which can be explained by the lack of nitrate supply as an N₂O precursor in reduced conditions and reduction of N₂O to N₂ during denitrification when the water table is high (Butterbach-Bahl et al. 2011; Voigt et al. 2017). Recent observations not included in the N₂O review dataset (Voigt et al 2020) show that wetlands may also function as net N₂O sinks in the Arctic (Schulze et al. 2023).

Table 1. Greenhouse gas (GHGs - CO₂, CH₄, and N₂O) budget for the permafrost region based on ecosystem upscaling. Negative GHG emissions represent an uptake while positive emissions represent a release. GHG emissions from terrestrial ecosystems are reported as mean fluxes with 2.5 and 97.5% confidence intervals (CI). GHG emissions from inland waters and fires are reported with 5 and 95% CI. GHG emissions from abrupt thaw are reported with +40% uncertainty range. *these fluxes are estimated using the abrupt thaw model from Turetsky et al (2020) and are considered as additive to the total for these categories (to avoid double counting of fluxes). **includes CO₂, CH₄ and lateral fluxes.

| | | Area | CO ₂ |
|---|---|---------------------------------|--|
| | | 10 ⁶ km ² | Tg CO ₂ -C yr ⁻¹ mean |
| Upland and wetland land covers | Upland and wetland land covers | 17.05 | -339.6 |
| | Boreal Forests | 9 | -270.3 |
| | Non-permafrost Wetlands | 1.6 | -69.4 |
| | Permafrost Bogs | 0.86 | -0.05 |
| | Dry Tundra | 5.2 | 2.9 |
| | Tundra Wetlands | 0.38 | -2.7 |
| <i>Subfraction from wetland abrupt thaw*</i> | <i>Subfraction from wetland abrupt thaw*</i> | <i>0.72</i> | 19.3 |
| <i>Subfraction from upland hillslope abrupt thaw*</i> | <i>Subfraction from upland hillslope abrupt thaw*</i> | <i>0.014</i> | 0.3 |
| Inland waters | Inland waters | 1.4 | 230.6 |
| | Rivers | 0.12 | 164.4 |
| | Lakes | 1.3 | 66.2 |
| <i>Subfraction from lowland abrupt thaw lakes*</i> | <i>Subfraction from lowland abrupt thaw lakes*</i> | 0.43 | 11.6 |
| Fires | | 1.1 | 109.4 |
| | Boreal | 0.96 | 100.0 |
| | Tundra | 0.11 | 9.4 |
| Geological emissions | Geological emissions | | NA |
| TOTAL GHG BUDGET | | | 0.36 |
| Lateral fluxes | | | 94 |
| | Riverine flux | | 78 |
| | Coastal erosion | | 15 |
| TOTAL C** AND N BUDGETS | | | 136.4 |

Table 2. Growing season (gs) emissions of Greenhouse gas (GHGs - CO₂, CH₄, and N₂O) from terrestrial ecosystems in the permafrost region. GHG emissions are reported as mean fluxes with 2.5 and 97.5% confidence intervals (CI). *non-permafrost wetlands include fens, bogs, and marshes. Due to lack of data, N₂O fluxes for non-permafrost wetlands, fluxes are assumed to be equal to those of tundra wetlands.

| | | Area | | CO ₂ | CO ₂ |
|--------------------------------|--------------------------------|---------------------------------|-----------|--|---|
| | | 10 ⁶ km ² | sites (#) | Tg CO ₂ -C yr ⁻¹ mean | Tg CO ₂ -C yr ⁻¹ 2.5% CI |
| Upland and wetland land covers | Upland and wetland land covers | 17.05 | 95 | -1611 | -2148 |
| | Boreal Forests | 9 | 25 | -1034 | -1305 |
| | Non-permafrost Wetlands | 1.6 | 10 | -145 | -193 |
| | Permafrost Bogs | 0.86 | 2 | -54 | -139 |
| | Dry Tundra | 5.2 | 25 | -358 | -482 |
| | Tundra Wetlands | 0.38 | 33 | -20 | -29 |

3.2 Net GHG emissions from inland waters

Inland aquatic ecosystems were a net source of CO₂ (230.6 (132.4, 359.8) Tg CO₂-C y⁻¹), CH₄ (9.4 (4.5, 13.1) Tg CH₄-C y⁻¹), and N₂O (0.0019 (0.0008, 0.0029) Tg N₂O-N y⁻¹). Rivers emitted annually 164.4 (107.3, 222.5) Tg CO₂-C y⁻¹, 2.3 (1.6, 2.9) Tg CH₄-C y⁻¹ and 0.0006 (0.0004, 0.0008) Tg N₂O-N y⁻¹ to the atmosphere. These high riverine fluxes are due to their supersaturation in CO₂ as they are receiving and degassing CO₂ derived from adjacent soils. To our knowledge, there are no specific annual estimates of riverine GHGs for the permafrost region to compare our estimates, however, when compared to emissions from high latitude, our methane emissions for rivers are within the lower range of published estimates (0.3-7.5 Tg CH₄-C y⁻¹) (Thornton et al. 2016).

In comparison to riverine emissions, lakes were a weaker source of CO₂ (66.2 (25.1, 137.3) Tg CO₂-C y⁻¹) but a stronger source of CH₄ (7.1 (2.9, 10.2) Tg CH₄ y⁻¹) and N₂O (0.0012 (0.0004, 0.002) Tg N₂O-N y⁻¹) (Table 1). Our annual lake CH₄ emission estimate is lower than previous estimates reported by Wik et al. (2016) (12.4 (7.3, 25.7) Tg CH₄-C y⁻¹) and Matthews et al. (2020) (13.8-17.7 Tg CH₄-C y⁻¹). This is partly related to the difference in lake classifications where in this study lakes were separated by both types and size categories, whereas these previous estimates separated the lakes by type alone- although domain sizes differ slightly. The largest source of lake CH₄ emissions were from small peatland lakes (~ 30% of lakes emissions, Table A3), which are dominant in the peat-rich regions of the Hudson Bay Lowlands in Canada and the West Siberian Lowland in western Russia (Olefeldt et al. 2021). However, the areas of small lakes estimated by BAWLD are among the most uncertain of the land cover classes (Olefeldt et al. 2021), due to limited spatial data used for lakes and great flux variability among small lakes across the domain (Muster et al. 2019). Our mean lake and river CO₂ emission estimates for the permafrost region constitute ~12% of reported global annual CO₂ emissions for lakes (Holgerson et al. 2016) and rivers (Liu et al. 2021). We note that there is a substantial lack of CH₄ flux data for Boreal-Arctic lakes (Stanley et al. 2016), making our estimates highly uncertain. While there is no estimate of N₂O emissions from arctic lakes, Kortelainen et al. (2020) estimated boreal lakes N₂O emissions at 0.029 (0.026, 0.032) Tg N₂O-N y⁻¹.

3.3 Net GHG emissions from disturbances: fires and abrupt thaw

Fires within the study region affected 1.1 x 10⁶ km² during the period 2000-2016. On average, fires impacted 0.06 million km² annually, emitting 109.4 (83.5, 135.3) Tg CO₂-C yr⁻¹, 1.2 (0.9, 1.5) Tg CH₄-C yr⁻¹, and 0.07 (0.06, 0.08) Tg N₂O-N yr⁻¹. Ninety percent of the annually burned area was in the boreal biome, contributing

to more than 92% of the permafrost region fire GHG emissions (Table 1). Fire CO₂ emissions offset a third of the CO₂ uptake from terrestrial ecosystems, while CH₄ and N₂O emissions from fires represented 5% and 13% of the CH₄ and N₂O emitted by terrestrial ecosystems, respectively. Our fire flux estimates mainly reflect direct emissions from combustion. There is also a component of increased growth during post-fire recovery, which we do not explicitly account for. However, it is indirectly accounted for as many of the in situ flux data were collected from previously burned ecosystems (which drives up the mean land cover flux). Our fire carbon emission estimate for boreal ecosystems (CO₂ and CH₄, 113.2 TgC yr⁻¹) is slightly lower than the one of 142 Tg CO₂-C yr⁻¹ previously reported by Veraverbeke et al. (2021). Using GFED4s data, our budget might underestimate fire CO₂ emissions as shown in Potter et al. (2022), where GFED4s emissions were 36% lower than the ones obtained using the ABoVE-FED data-driven product.

The total area affected by active and stabilised abrupt thaw between 2000 and 2020 was estimated to be 1.2 x 10⁶ km² (0.43 x 10⁶ in lowlands, 0.01 x 10⁶ in uplands, and 0.72 x 10⁶ in wetlands), accounting for ca. 7% of the permafrost region (Table 1). All together, areas affected by abrupt thaw were net emitters of 31 (21, 42) Tg CO₂-C yr⁻¹ and 31 (20, 42) Tg CH₄-C yr⁻¹ (Table 1, details in Table A6). CO₂ and CH₄ emissions from wetland abrupt thaw were the largest. GHG estimates from abrupt thaw were not directly included in the permafrost GHG budget as it was not possible to know how much were already accounted for in the budget from terrestrial upscaling. Yet, the impact of abrupt thaw processes on C cycling in the permafrost region is large, and it is projected that it will contribute nearly as much as gradual thaw to future radiative forcing from permafrost thaw (Turetsky et al. 2020).

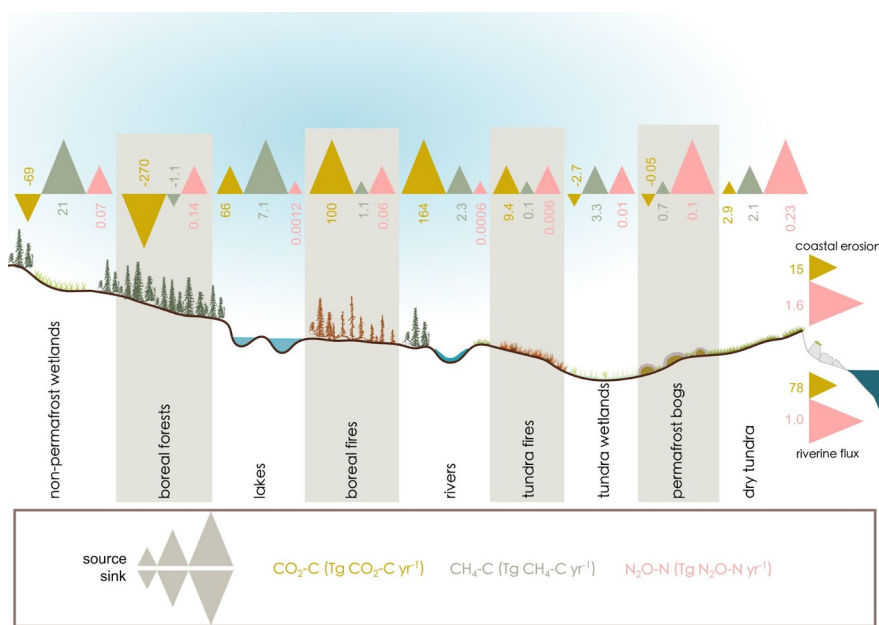


Figure 3: Scheme of annual atmospheric GHGs exchange (CO₂, CH₄, and N₂O) for the five terrestrial land cover classes (Boreal Forests, Non-permafrost Wetlands, Dry Tundra, Tundra Wetlands and Permafrost Bogs); inland water classes (Rivers and Lakes). Annual lateral fluxes from coastal erosion and riverine fluxes are also reported in Tg C yr⁻¹ and Tg N yr⁻¹. Symbols for fluxes indicate high ($x > Q3$), medium ($Q1 < x < Q3$), and low ($< Q1$) fluxes, in comparison the quartile (Q). Note that the magnitudes across three different GHG fluxes within each land cover class cannot be compared with each other.

3.4 Total GHGs, C, and N budgets

Summing up all budget components, the permafrost region was a source of GHGs throughout the period 2000-2020 (Table 1). Emissions of CO₂ were weak with 0.36 (-619.7, 651.5) Tg CO₂-C yr⁻¹ due to the large CO₂ uptake from terrestrial ecosystems. Emissions from aquatic ecosystems were the largest source of CO₂ annually. CH₄ and N₂O emissions were 37.7 (21.3, 52.8) Tg CH₄-C yr⁻¹ and 0.62 (0.03, 1.19) Tg N₂O-N yr⁻¹, respectively with terrestrial ecosystems as largest contributors (68 and 89%, respectively). Lateral fluxes were 94 (79, 111) Tg C yr⁻¹ and 2.6 Tg N yr⁻¹ (Table 1), riverine flux contributing 83 and 38%, respectively.

Taking into account all the above mentioned budget components, the total C (including atmospheric CO₂, CH₄, and lateral fluxes) budget for the permafrost region between 2000- 2020 were estimated to 136.4 (-516.7, 820.5) Tg C yr⁻¹. Close to 70% of the C released from the permafrost region was through lateral fluxes with 57% being released through coastal erosion. Atmospheric CO₂ contributed ca. 1% to the total C released from the region while atmospheric CH₄ contributed 31%. The total N budget for the permafrost region was 3.2 (1.9, 4.8) Tg N yr⁻¹. Most of (81%) the N released was through lateral fluxes with coastal erosion releasing 50% of the total N from the region. Atmospheric N₂O from inland waters was negligible while atmospheric N₂O from terrestrial ecosystems represented 17% of the total N released in the permafrost region. Atmospheric N₂O losses due to fires represented 2% of the N in the permafrost region.

3.5 Main sources of uncertainty and research directions

Limitations in the number of observations

A major challenge in the representation of GHG exchange in high-latitude and remote environments relates to limitations in spatial representation, length and quality of observational time series (Pallandt et al. 2022, Virkkala et al. 2018). The synthesis datasets used here to estimate GHGs fluxes are the most comprehensive ones currently available and have been significantly growing during the past decade. However, more observations covering the full annual cycles are still needed to improve the representativeness of heterogeneous and underrepresented landscapes and climatic conditions. Specifically, more observations from the dry tundra land cover class are needed to verify its GHG sink-source status and from ecosystems experiencing disturbances such as abrupt thaw. CH₄ flux measurements are limited in boreal forests, and N₂O flux measurements are scarce for all terrestrial and aquatic ecosystems. Across all the GHG fluxes, measurements in environments with low fluxes are also important to avoid biasing our understanding to hotspot regions. Limitations related to the number of flux measurements could be overcome by increasing in situ and laboratory manipulation studies. This would improve process-based understanding of fluxes and their response to changes in temperature, moisture, permafrost thaw and other disturbances. Improvements in the reporting of measurements and metadata should be prioritised for a better integration of available data, especially to address reporting of net-zero or negative fluxes. Difficulties in measuring small exchange rates can be overcome by using new technologies based on portable, high-precision laser instruments (e.g., Juncher Jørgensen et al. 2015, D’Imperio et al. 2017, Juutinen et al. 2022). Very recently, such portable high-precision instruments are becoming available also for N₂O, opening possibilities for more numerous and accurate N₂O flux estimates, including capturing of N₂O uptake.

N₂O flux measurements from inland waters are still scarce and ice-out estimates are often missing for CH₄ fluxes. Moreover, seasonally inundated water bodies are not well represented although they might contribute substantially to the release of GHGs in short periods of time.

Estimates of high latitude lateral fluxes of C and N are fairly well constrained in comparison to land-atmosphere GHG fluxes. However, available estimates are provided for the major six largest arctic rivers

that represent 50% of the total area covered by rivers (Speetjens et al. 2023). Although smaller catchments are highly abundant, estimates of GHG fluxes are not well constrained for the permafrost region. Improving this understanding will allow lateral flux integration of these smaller catchments in the main estimates of lateral fluxes from inland waters.

Limitations related to the land cover classification

Differences in GHG fluxes among land cover classes are large. Therefore, it is crucial to get their representation correctly to improve land cover-based GHG flux upscaling. To date, there is no accurate land cover classification of permafrost landscapes (both dry and wet) at a circumpolar scale. We used the BAWLD land cover classification (Olefeldt et al. 2021) in which land cover classes were defined to enable upscaling of CH₄ fluxes at large spatial scales. While very relevant to facilitate large-scale mapping of CH₄ fluxes it lacks sufficient classes to allow separation among groups of dryer ecosystems that might have large variability in CO₂ or N₂O fluxes. This is the case for the dry tundra and boreal forest classes that comprise a mosaic of ecosystems with different vegetation types. This results in a large uncertainty range in the class flux estimate of the dry tundra (see Table 1, Table A5), making the interpretation of the flux estimates difficult.

Emissions from small water bodies (<0.1 km²) globally represent important inland water CO₂ and CH₄ fluxes (Holgerson and Raymond, 2016) and even more at high latitudes. Although accounted for in this study, emissions from small water bodies are quite uncertain as they are difficult to map at a large scale due to their high temporal and spatial variability. Small ponds and lakes can be temporary and their size can vary depending on the amount of precipitation after snowmelt; they expand much in wet years and after snowmelt and can often disappear in dry years or late in summer. Improving the spatial and temporal resolution of the products used to map inland waters would benefit the representation of small water bodies, which would resolve a critical source of uncertainty in calculating GHGs exchange.

Limited understanding on the impact of disturbances on the GHG budget

As ecosystems go through disturbance cycles, there are both losses and gains of C and N to ecosystems. It is unclear how well post-disturbance dynamics, e.g. post-fire regrowth, is captured in our ecosystem flux upscaling. Updated budgets need to consider new datasets of fire emissions to cover the period post-2016 as well as post-fire recovery processes. Our emissions from fires consider direct GHG emissions but not the indirect and longer-term soil emissions resulting from fire-induced ground thaw. Although carbon losses might be offset by shifts in species composition (Randerson et al. 2006; Ueyama et al. 2019; Mack et al. 2021), fires can also initiate further permafrost thaw and degradation (Genet et al. 2013; Jafarov et al. 2013; Gibson et al. 2018). As such, fires can trigger shifts in the landscapes, impacting biogeochemical cycling (Randerson et al. 2006; Bouskill et al. 2022; Hermesdorf et al. 2022; Köster et al. 2018b; Ullah et al. 2009; Abbott and Jones, 2015; Voigt et al. 2017; Marushchak et al. 2021; Wilkerson et al. 2019). Improving our understanding of landscape transitions due to fire will help constrain the contribution of disturbances to the GHG budget.

The spatial extent and GHG emissions from abrupt thaw disturbances remain poorly constrained due to a lack of available data (Turetsky et al. 2020). Flux measurements from abrupt thaw are still scarce and thus their reported flux estimate should be interpreted carefully. Improving the numbers of in situ measurements from abrupt thaw disturbances and consistent reporting should be a key to understanding the impact of abrupt thaw on permafrost GHG budgets. Transition rates (from active to stabilised abrupt thaw feature) need to be further understood and systematic mapping of abrupt thaw areas remain to be improved to better constrain emissions from abrupt thaw. N₂O emissions from abrupt thaw were not included in this study due to the small number of observations reported in the literature and little understanding on the impact of abrupt thaw on emissions N₂O. It was shown that such disturbances frequently cause N₂O emission hotspots

(Voigt et al. 2020) with two recent studies using a terrestrial ecosystem model simulate enhanced gaseous N losses from thawing permafrost (Lacroix et al. 2022; Yuan et al. 2023). However, another study shows that atmospheric uptake of N₂O in peat plateaus and thermokarst bogs increased with soil temperature and soil moisture following disturbances (Schulze et al. 2023). Local hydrology will determine whether the site will turn into a source of N₂O after thaw, as high emissions can occur at intermediate moisture conditions in N rich soils (Marushchak et al. 2021) but a transition to wetland would promote denitrification with N₂ as the final product and prevent N₂O release (Voigt et al. 2017; Butterbach-Bahl and Dannenmann 2011) or even cause or enhance net N₂O uptake (Schulze et al. 2023).

As our understanding of processes leading to GHG release through abrupt thaw is constantly improving, future permafrost GHG budgets will be able to better integrate both atmospheric and lateral fluxes from abrupt thaw. So far, the abrupt thaw model (Turestky et al. 2020) does not consider lateral fluxes from abrupt thaw. While we might capture these losses through our lateral fluxes budget, future budgets should allow measuring the fraction of what is lost due to abrupt thaw. Other disturbances including anthropogenic disturbances (e.g. clear cutting and logging) have not been estimated in this study. Future budgets could aim at constraining the impact of these disturbances on the permafrost GHG budget.

5 Conclusions

Using a land cover-based ecosystem flux upscaling approach (including fluxes from terrestrial ecosystems, inland water, disturbances and geological fluxes), the permafrost region was identified as an annual source of GHGs between 2000-2020. The region emitted 0.36 (-620, 652) Tg CO₂-C y⁻¹ (mean and 95% confidence interval range used hereafter), 42 (24, 58) Tg CH₄-C y⁻¹, and 0.62 (0.03, 1.2) Tg N₂O-N y⁻¹ to the atmosphere. The region was thus a net source of CH₄ and N₂O. For CO₂, although the 20-year mean is a net source, the uncertainty range remains large, extending from a large sink to an even larger source of CO₂ and, therefore, challenging the calculation of the net flux sign. We suggest that terrestrial ecosystems were likely an ecosystem CO₂ sink, but emissions from disturbances and inland waters offset this flux, making the full CO₂ budget largely indistinguishable from zero (neutral). The total C (including atmospheric CO₂, CH₄, and lateral fluxes) and N budget for the permafrost region were estimated to 136 (-517, 821) Tg C y⁻¹ and 3.2 (1.9, 4.8) Tg N y⁻¹.

Acknowledgments

This work is a collaborative effort from the Global Carbon Project Second REgional Carbon Cycle and Processes study (RECCAP2) and contributes to the Arctic Methane and Permafrost Challenge (AMPAC). JR and GH acknowledge support from the European Union's Horizon 2020 Research and Innovation Programme to the Nunataryuk project (no. 773421) and support from the AMPAC-Net project funded by the European Space Agency (ESA). JR received additional funding from the Swedish Academy of Science (Formas) under the grant number FR-2021/0004. EJB has received funding from the European Union's Horizon 2020 research and innovation programme under Grant Agreement No 101003536 (ESM2025 - Earth System models for the Future) and from the Joint UK BEIS/Defra Met Office Hadley Centre Climate Programme (GA01101). Work of MEM was supported by the Academy of Finland in the frame of the Atmosphere and Climate Competence Center (ACCC) (no. 337550). CV was supported by the Academy of Finland project MUFFIN (grant no. 332196). CB wishes to thank the Academy of Finland (project N-PERM - decision no. 341348, project NOCA - decision no. 314630 and the Yedoma-N project decision no. 287469) for financial support.

AMV, BMR, SMN, JDW, and SP were funded by the Gordon and Betty Moore foundation (grant #8414) and through funding catalyzed by the Audacious Project (Permafrost Pathways). MAK was supported by the NSF PRFB Program (Abstract # 2109429). TK acknowledges support through the project Palmod, funded by the German Federal Ministry of Education and Research (BMBF), Grant No. 01LP1921A. JGC was funded by the Australian National Environmental Science Program (NESP2) - Climate Systems Hub. MIROC4-ACTM inversion activity is supported by the Arctic Challenge for Sustainability phase II (ArCS-II; JPMXD1420318865) Projects of the Ministry of Education, Culture, Sports, Science and Technology (MEXT), and Environment Research and Technology Development Fund (JPMEERF21S20800) of the Environmental Restoration and Conservation Agency of Japan. ELB considers this study a contribution to GreenFeedBack (Greenhouse gas fluxes and earth system feedbacks) funded by the European Union's HORIZON research and innovation program under grant agreement No 101056921. EAGS was funded by NSF PLR Arctic System Science Research Networking Activities (RNA) Permafrost Carbon Network: Synthesizing Flux Observations for Benchmarking Model Projections of Permafrost Carbon Exchange (2019-2023) Grant#1931333.

References

- Abbott, B.W. and Jones, J.B., 2015. Permafrost collapse alters soil carbon stocks, respiration, CH₄, and N₂O in upland tundra. *Global Change Biology*, 21(12), pp.4570-4587.
- Biskaborn, B.K., Smith, S.L., Noetzli, J., Matthes, H., Vieira, G., Streletskiy, D.A., Schoeneich, P., Romanovsky, V.E., Lewkowitz, A.G., Abramov, A. and Allard, M., 2019. Permafrost is warming at a global scale. *Nature communications*, 10(1), pp.1-11.
- Bouskill, N.J., Mekonnen, Z., Zhu, Q., Grant, R. and Riley, W.J., 2022. Microbial contribution to post-fire tundra ecosystem recovery over the 21st century. *Communications Earth & Environment*, 3 (1), p.26.
- Burke, E. J., Ekici, A., Huang, Y., Chadburn, S. E., Huntingford, C., Ciais, P., Friedlingstein, P., Peng, S., and Krinner, G.: Quantifying uncertainties of permafrost carbon-climate feedbacks, *Biogeosciences*, 14, 3051–3066, <https://doi.org/10.5194/bg-14-3051-2017>, 2017.
- Burke, E., Chadburn, S. and Huntingford, C., 2022. Thawing permafrost as a nitrogen fertiliser: Implications for climate feedbacks. *Nitrogen*, 3(2), pp.353-375.
- Butterbach-Bahl, K. and Dannenmann, M., 2011. Denitrification and associated soil N₂O emissions due to agricultural activities in a changing climate. *Current Opinion in Environmental Sustainability*, 3 (5), pp.389-395.
- Chen, Y., Liu, F., Kang, L., Zhang, D., Kou, D., Mao, C., Qin, S., Zhang, Q. and Yang, Y., 2021. Large-scale evidence for microbial response and associated carbon release after permafrost thaw. *Global Change Biology*, 27(14), pp.3218-3229.
- Christensen, T.R., Lund, M., Skov, K. et al. Multiple Ecosystem Effects of Extreme Weather Events in the Arctic. *Ecosystems* 24, 122–136 (2021). <https://doi.org/10.1007/s10021-020-00507-6>
- Ciais, P., Bastos, A., Chevallier, F., Lauerwald, R., Poulter, B., Canadell, P., Hugelius, G., Jackson, R.B., Jain, A., Jones, M. and Kondo, M., 2022. Definitions and methods to estimate regional land carbon fluxes for the second phase of the REgional Carbon Cycle Assessment and Processes Project (RECCAP-2). *Geoscientific Model Development*, 15(3), pp.1289-1316.
- Chadburn, S., Burke, E., Cox, P. et al. An observation-based constraint on permafrost loss as a function of global warming. *Nature Clim Change* 7, 340–344 (2017). <https://doi.org/10.1038/nclimate3262>
- Cole, J.J., Prairie, Y.T., Caraco, N.F., McDowell, W.H., Tranvik, L.J., Striegl, R.G., Duarte, C.M., Korteinainen, P., Downing, J.A., Middelburg, J.J. and Melack, J., 2007. Plumbing the global carbon cycle:

integrating inland waters into the terrestrial carbon budget. *Ecosystems* ,10 , pp.172-185.

Edwards M, Langdon C. Holocene thermokarst lake dynamics in northern interior Alaska: the interplay of climate, fire, and subsurface hydrology. *Front Earth Sci.* 2019;7(53):1-22.

Friedlingstein, P., Jones, M.W., O'Sullivan, M., Andrew, R.M., Bakker, D.C., Hauck, J., Le Quere, C., Peters, G.P., Peters, W., Pongratz, J. and Sitch, S., 2022. Global carbon budget 2021. *Earth System Science Data* , 14 (4), pp.1917-2005.

Genet, H., McGuire, A. D., Barrett, K., Breen, A., Euskirchen, E. S., Johnstone, J. F., et al. (2013). Modeling the effects of fire severity and climate warming on active layer thickness and soil carbon storage of black spruce forests across the landscape in interior Alaska. *Environmental Research Letters*, 8(4), 045016. <https://doi.org/10.1088/1748-9326/8/4/045016>

Gibson, C.M., Chasmer, L.E., Thompson, D.K., Quinton, W.L., Flannigan, M.D. and Olefeldt, D., 2018. Wildfire as a major driver of recent permafrost thaw in boreal peatlands. *Nature communications* ,9 (1), p.3041.

Grosse, G., Harden, J., Turetsky, M., McGuire, A.D., Camill, P., Tarnocai, C., Froking, S., Schuur, E.A., Jorgenson, T., Marchenko, S. and Romanovsky, V., 2011. Vulnerability of high-latitude soil organic carbon in North America to disturbance. *Journal of Geophysical Research: Biogeosciences*, 116(G4).

Hermesdorf, L., Elberling, B., D'Imperio, L., Xu, W., Lambaek, A. and Ambus, P.L., 2022. Effects of fire on CO₂, CH₄ and N₂O exchange in a well-drained Arctic heath ecosystem. *Global Change Biology* .

Holgerson, M.A. and Raymond, P.A., 2016. Large contribution to inland water CO₂ and CH₄ emissions from very small ponds. *Nature Geoscience*, 9(3), pp.222-226.

Holloway, J.E., Lewkowicz, A.G., Douglas, T.A., Li, X., Turetsky, M.R., Baltzer, J.L. and Jin, H., 2020. Impact of wildfire on permafrost landscapes: A review of recent advances and future prospects. *Permafrost and Periglacial Processes*, 31(3), pp.371-382.

Humborg, C., Morth, C.M., Sundbom, M., Borg, H., Blenckner, T., Giesler, R. and Ittekkot, V., 2010. CO₂ supersaturation along the aquatic conduit in Swedish watersheds as constrained by terrestrial respiration, aquatic respiration and weathering. *Global Change Biology*, 16(7), pp.1966-1978.

IPCC, 2022: Climate Change 2022: Mitigation of Climate Change. Contribution of Working Group III to the Sixth Assessment Report of the Intergovernmental Panel on Climate Change [P.R. Shukla, J. Skea, R. Slade, A. Al Khouradajie, R. van Diemen, D. McCollum, M. Pathak, S. Some, P. Vyas, R. Fradera, M. Belkacemi, A. Hasija, G. Lisboa, S. Luz, J. Malley, (eds.)]. Cambridge University Press, Cambridge, UK and New York, NY, USA. doi: 10.1017/9781009157926

Jafarov, E. E., Romanovsky, V. E., Genet, H., McGuire, A. D., & Marchenko, S. S. (2013). The effects of fire on the thermal stability of permafrost in lowland and upland black spruce forests of interior Alaska in a changing climate. *Environmental Research Letters*, 8(3), 035030. <https://doi.org/10.1088/1748-9326/8/3/035030>

Kim, Y., and Tanaka, N., Effect of forest fire on the fluxes of CO₂, CH₄, and N₂O in boreal forest soils, interior Alaska, *J. Geophys. Res.* , 108(D1), 8154, doi:10.1029/2001JD000663, 2003.

Kortelainen, P, Larmola, T, Rantakari, M, Juutinen, S, Alm, J, Martikainen, PJ. Lakes as nitrous oxide sources in the boreal landscape. *Glob Change Biol* . 2020; 26: 1432– 1445. <https://doi.org/10.1111/gcb.14928>

Koster, K., Koster, E., Berninger, F., Heinonsalo, J. and Pumpanen, J., 2018a. Contrasting effects of reindeer grazing on CO₂, CH₄, and N₂O fluxes originating from the northern boreal forest floor. *Land Degradation & Development* , 29 (2), pp.374-381.

Koster, E., Koster, K., Berninger, F., Prokushkin, A., Aaltonen, H., Zhou, X. and Pumpanen, J., 2018b. Changes in fluxes of carbon dioxide and methane caused by fire in Siberian boreal forest with continuous permafrost. *Journal of environmental management*, 228, pp.405-415.

- Kuhn, M.A., Varner, R.K., Bastviken, D., Crill, P., MacIntyre, S., Turetsky, M., Walter Anthony, K., McGuire, A.D. and Olefeldt, D., 2021a. BAWLD-CH4: A Comprehensive Dataset of Methane Fluxes from Boreal and Arctic Ecosystems. *Earth System Science Data Discussions*, pp.1-56.
- Kuhn, M. A., Thompson, L. M., Winder, J. C., Braga, L. P. P., Tanentzap, A. J., Bastviken, D., & Olefeldt, D. 2021b. Opposing effects of climate and permafrost thaw on CH₄ and CO₂ emissions from northern lakes. *AGU Advances* , 2, e2021AV000515. <https://doi.org/10.1029/2021AV000515>
- Kuhn, M.A., Thompson, L.M., Winder, J.C., Braga, L.P., Tanentzap, A.J., Bastviken, D. and Olefeldt, D., 2021c. Opposing effects of climate and permafrost thaw on CH₄ and CO₂ emissions from northern lakes. *AGU Advances*, 2(4), p.e2021AV000515.
- Lacroix, F., Zaehle, S., Caldararu, S., Schaller, J., Stimmler, P., Holl, D., Kutzbach, L. and Gockede, M., 2022. Mismatch of N release from the permafrost and vegetative uptake opens pathways of increasing nitrous oxide emissions in the high Arctic. *Global Change Biology* .
- Lantuit, H. et al. (2012). The Arctic Coastal Dynamics database: a new classification scheme and statistics on Arctic permafrost coastlines. *Estuaries Coasts* 35, 383–400.
- Lauerwald, R., Regnier, P., Figueiredo, V., Enrich-Prast, A., Bastviken, D., Lehner, B., et al. (2019). Natural lakes are a minor global source of N₂O to the atmosphere. *Global Biogeochemical Cycles*, 33,1564-1581, <https://doi.org/10.1029/2019GB006261>
- Li, G., Zhang, M., Pei, W., Melnikov, A., Khristoforov, I., Li, R. and Yu, F., 2022. Changes in permafrost extent and active layer thickness in the Northern Hemisphere from 1969 to 2018. *Science of The Total Environment*, 804, p.150182.
- Liu, Z., Kimball, J.S., Ballantyne, A.P., Parazoo, N.C., Wang, W.J., Bastos, A., Madani, N., Natali, S.M., Watts, J.D., Rogers, B.M. and Ciais, P., 2022. Respiratory loss during late-growing season determines the net carbon dioxide sink in northern permafrost regions. *Nature communications*, 13(1), pp.1-13., <https://www.nature.com/articles/s41467-022-33293-x>
- Liu, S., Kuhn, C., Amatulli, G., Aho, K., Butman, D.E., Allen, G.H., Lin, P., Pan, M., Yamazaki, D., Brinkerhoff, C. and Gleason, C., 2022. The importance of hydrology in routing terrestrial carbon to the atmosphere via global streams and rivers. *Proceedings of the National Academy of Sciences* , 119 (11), p.e2106322119.
- Lopez-Blanco, E., Langen, P. L., Williams, M., Christensen, J. H., Boberg, F., Langley, K., and Christensen, T. R. (2022). The future of tundra carbon storage in Greenland – Sensitivity to climate and plant trait changes. *Science of The Total Environment* , 157385. <https://doi.org/10.1016/j.scitotenv.2022>
- Maavara, T., Lauerwald, R., Laruelle, G., Akbarzadeh, Z., Bouskill, N., Van Cappellen, P., & Regnier, P. (2019). Nitrous oxide emissions from inland waters: Are IPCC estimates too high? *Global Change Biology*, 25(2), 473–488. <https://doi.org/10.1111/gcb.14504>
- Mack, M.C., Walker, X.J., Johnstone, J.F., Alexander, H.D., Melvin, A.M., Jean, M. and Miller, S.N., 2021. Carbon loss from boreal forest wildfires offset by increased dominance of deciduous trees. *Science*, 372(6539), pp.280-283.
- Marushchak, M.E., Pitkamaki, A., Koponen, H., Biasi, C., Seppala, M. and Martikainen, P.J., 2011. Hot spots for nitrous oxide emissions found in different types of permafrost peatlands. *Global Change Biology*, 17(8), pp.2601-2614.
- Marushchak, M.E., Kerttula, J., Diakova, K. et al., 2021. Thawing Yedoma permafrost is a neglected nitrous oxide source. *Nat Commun* 12, 7107. <https://doi.org/10.1038/s41467-021-27386-2>
- Matson, A., Pennock, D. and Bedard-Haughn, A., 2009. Methane and nitrous oxide emissions from mature

forest stands in the boreal forest, Saskatchewan, Canada. *Forest Ecology and Management* ,258 (7), pp.1073-1083.

Matthews, E., Johnson, M.S., Genovese, V., Du, J. and Bastviken, D., 2020. Methane emission from high latitude lakes: methane-centric lake classification and satellite-driven annual cycle of emissions. *Scientific Reports*, 10(1), pp.1-9.

McGuire, A.D., Christensen, T.R., Hayes, D., Heroult, A., Euskirchen, E., Kimball, J.S., Koven, C., Lafleur, P., Miller, P.A., Oechel, W. and Peylin, P., 2012. An assessment of the carbon balance of Arctic tundra: comparisons among observations, process models, and atmospheric inversions. *Biogeosciences* , 9 (8), pp.3185-3204.

Miner, K.R., Turetsky, M.R., Malina, E. et al. Permafrost carbon emissions in a changing Arctic. *Nat Rev Earth Environ* 3, 55–67 (2022). <https://doi.org/10.1038/s43017-021-00230-3>

Morishita, T., Hatano, R., and Desyatkin, R.V., 2007. N2O Flux in Alas Ecosystems Formed by Forest Disturbance Near Yakutsk, Eastern Siberia, Russia. *Eurasian Journal of Forest Research* , 10 (1), pp.79-84.

Morner, N.-A. and Etiope, G. (2002) Carbon degassing from the lithosphere, *Global Planet. Change*, 33, 185–203.

Muster, S., Riley, W.J., Roth, K., Langer, M., Cresto Aleina, F., Koven, C.D., Lange, S., Bartsch, A., Grosse, G., Wilson, C.J. and Jones, B.M., 2019. Size distributions of Arctic waterbodies reveal consistent relations in their statistical moments in space and time. *Frontiers in Earth Science*, p.5.

Natali, S.M., Watts, J.D., Rogers, B.M. et al. Large loss of CO₂ in winter observed across the northern permafrost region. *Nat. Clim. Chang.* 9, 852–857 (2019). <https://doi.org/10.1038/s41558-019-0592-8>

Natali, S.M., Holdren, J.P., Rogers, B.M., Treharne, R., Duffy, P.B., Pomerance, R. and MacDonald, E., 2021. Permafrost carbon feedbacks threaten global climate goals. *Proceedings of the National Academy of Sciences*, 118(21).

Obu, J.; Westermann, S.; Barboux, C.; Bartsch, A.; Delaloye, R.; Grosse, G.; Heim, B.; Hugelius, G.; Irrgang, A.; Kaab, A.M.; Kroisleitner, C.; Matthes, H.; Nitze, I.; Pellet, C.; Seifert, F.M.; Strozzi, T.; Wegmuller, U.; Wiczorek, M.; Wiesmann, A. (2021): ESA Permafrost Climate Change Initiative (Permafrost_cci): Permafrost extent for the Northern Hemisphere, v3.0. NERC EDS Centre for Environmental Data Analysis, 28 June 2021. <http://dx.doi.org/10.5285/6e2091cb0c8b4106921b63cd5357c97c>

Olefeldt, D., Hovemyr, M., Kuhn, M.A., Bastviken, D., Bohn, T.J., Connolly, J., Crill, P., Euskirchen, E.S., Finkelstein, S.A., Genet, H. and Grosse, G., 2021. The Boreal–Arctic Wetland and Lake Dataset (BAWLD). *Earth system science data*, 13(11), pp.5127-5149.

Pallandt, M.M., Kumar, J., Mauritz, M., Schuur, E.A., Virkkala, A.M., Celis, G., Hoffman, F.M. and Gockede, M., 2022. Representativeness assessment of the pan-Arctic eddy covariance site network and optimized future enhancements. *Biogeosciences* , 19 (3), pp.559-583.

Palmtag, J., Obu, J., Kuhry, P., Richter, A., Siewert, M.B., Weiss, N., Westermann, S. and Hugelius, G., 2022. A high-spatial resolution soil carbon and nitrogen dataset for the northern permafrost region, based on circumpolar land cover upscaling. *Earth System Science Data Discussions* , pp.1-28.

Peltola, O., Vesala, T., Gao, Y., Raty, O., Alekseychik, P., Aurela, M., Chojnicki, B., Desai, A.R., Dolman, A.J., Euskirchen, E.S. and Friborg, T., 2019. Monthly gridded data product of northern wetland methane emissions based on upscaling eddy covariance observations. *Earth System Science Data* , 11 (3), pp.1263-1289.

Potter, S., Cooperdock, S., Veraverbeke, S., Walker, X., Mack, M. C., Goetz, S. J., Baltzer, J., Bourgeau-Chavez, L., Burrell, A., Dieleman, C., French, N., Hantson, S., Hoy, E. E., Jenkins, L., Johnstone, J. F., Kane, E. S., Natali, S. M., Randerson, J. T., Turetsky, M. R., Whitman, E., Wiggins, E., and Rogers,

- B. M.: Burned Area and Carbon Emissions Across Northwestern Boreal North America from 2001–2019, *EGUsphere*, <https://doi.org/10.5194/egusphere-2022-364>, 2022.
- Randerson, J.T., Liu, H., Flanner, M.G., Chambers, S.D., Jin, Y., Hess, P.G., Pfister, G., Mack, M.C., Treseder, K.K., Welp, L.R. and Chapin, F.S., 2006. The impact of boreal forest fire on climate warming. *science*, 314(5802), pp.1130-1132.
- Rantanen, M., Karpechko, A.Y., Lipponen, A. et al. The Arctic has warmed nearly four times faster than the globe since 1979. *Commun Earth Environ* 3, 168 (2022). <https://doi.org/10.1038/s43247-022-00498-3>
- Rocher-Ros, G., Giesler, R., Lundin, E., Salimi, S., Jonsson, A. and Karlsson, J., 2017. Large lakes dominate CO2 evasion from lakes in an Arctic catchment. *Geophysical Research Letters* , 44 (24), pp.12-254.
- Rodenhizer, H, Schuur, EAG et al. 2022. Abrupt Permafrost Thaw Accelerates Carbon Dioxide and Methane Release at a Tussock Tundra Site. *Arctic and Alpine Research*, in press.
- Runge, A., Nitze, I. and Grosse, G., 2022. Remote sensing annual dynamics of rapid permafrost thaw disturbances with LandTrendr. *Remote Sensing of Environment* , 268 , p.112752.
- Schulze, C., Sonnentag, O., Voigt, C., Thompson, L., van Delden, L., Heffernan, L., et al. (2023). Nitrous oxide fluxes in permafrost peatlands remain negligible after wildfire and thermokarst disturbance. *Journal of Geophysical Research: Biogeosciences* , 128, e2022JG007322. <https://doi.org/10.1029/2022JG007322>
- Schuur, E.A.G., J. Bockheim, J. Canadell, E. Euskirchen, C.B. Field, S.V Goryachkin, S. Hagemann, P. Kuhry, P. Lafleur, H. Lee, G. Mazhitova, F. E. Nelson, A. Rinke, V. Romanovsky, N. Shiklomanov, C. Tarnocai, S. Venevsky, J. G. Vogel, S.A. Zimov. 2008. Vulnerability of permafrost carbon to climate change: Implications for the global carbon cycle. *BioScience* 58: 701-714.
- Schuur, E.A.G., J.G. Vogel, K.G. Crummer, H. Lee, J.O. Sickman, and T.E. Osterkamp. 2009. The effect of permafrost thaw on old carbon release and net carbon exchange from tundra. *Nature* 459: 556-559. DOI: 10.1038/nature08031.
- Schuur, E.A.G., B.W. Abbott, W.B. Bowden, V. Brovkin, P. Camill, J.P. Canadell, F.S. Chapin III, T.R. Christensen, J.P. Chanton, P. Ciais, P.M. Crill, B.T. Crosby, C.I. Czimczik, G. Grosse, D.J. Hayes, G. Hugelius, J.D. Jastrow, T. Kleinen, C.D. Koven, G. Krinner, P. Kuhry, D.M. Lawrence, S.M. Natali, C.L. Ping, A. Rinke, W.J. Riley, V.E. Romanovsky, A.B.K. Sannel, C. Schadel, K. Schaefer, Z.M. Subin, C. Tarnocai, M. Turetsky, K. M. Walter-Anthony, C.J. Wilson, and S.A. Zimov. 2011. High risk of permafrost thaw. *Nature* 480:32-33.
- Schuur E.A.G., A.D. McGuire, G. Grosse, J.W. Harden, D.J. Hayes, G. Hugelius, C.D, Koven, P. Kuhry, D.M. Lawrence, S.M. Natali, D. Olefeldt, V.E. Romanovsky, C. Schadel, K. Schaefer, M. Turetsky, C. Treat, and J.E. Vonk. 2015. Climate change and the permafrost carbon feedback. *Nature* 520, 171–179.
- Schuur, E. A. G., A. D. McGuire, V. Romanovsky, C. Schadel, and M. Mack, 2018: Chapter 11: Arctic and boreal carbon. In *Second State of the Carbon Cycle Report (SOCCR2): A Sustained Assessment Report* [Cavallaro, N., G. Shrestha, R. Birdsey, M. A. Mayes, R. G. Najjar, S. C. Reed, P. Romero-Lankao, and Z. Zhu (eds.)]. U.S. Global Change Research Program, Washington, DC, USA, pp. 428-468, <https://doi.org/10.7930/SOCCR2.2018.Ch11>.
- Schuur, EAG, Bracho, R, Celis, G, Belshe, EF, Ebert, C, Ledman, J, M Mauritz, EF Pegoraro, C Plaza, H Rodenhizer, V Romanovsky, Christina S, D Schirokauer, M Taylor, JG Vogel, EE Webb 2021. Tundra underlain by thawing permafrost persistently emits carbon to the atmosphere over 15 years of measurements. *Journal of Geophysical Research: Biogeosciences*, 126, e2020JG006044. <https://doi.org/10.1029/2020JG006044>
- Schuur, E.A.G. 2020. Permafrost carbon [in “State of the Climate in 2019”]. *Bull. Amer. Meteor. Soc.* , 101 (8), S263–S265, <https://doi.org/10.1175/BAMS-D-20-0086.1>.

- Schuur, E.A.G., B. Abbott, R. Commane, J. Ernakovich, E. Euskirchen, G. Hugelius, G. Grosse, M. Jones, C. Koven, V. Leyshk, D. Lawrence, M. Lorant, M. Mauritz, D. Olefeldt, S. Natali, H. Rodenhizer, V. Salmon, C. Schaedel, J. Strauss, C. Treat, and M. Turetsky. 2022. Permafrost and climate change: Carbon cycle feedbacks from a warming Arctic. *Annual Reviews of Environment and Resources* 47:28.1-28.29 <https://doi.org/10.1146/annurev-environ-012220-011847>
- Schuur, E.A.G., and M.C. Mack. 2018. Ecological response to permafrost thaw and consequences for local and global ecosystem services. *Annual Reviews of Ecology, Evolution, and Systematics*. 49: 279-301.
- Serikova, S., Pokrovsky, O.S., Ala-Aho, P. et al. High riverine CO₂ emissions at the permafrost boundary of Western Siberia. *Nature Geosci* 11, 825–829 (2018). <https://doi.org/10.1038/s41561-018-0218-1>
- Simpson, I. J., Edwards, G. C., Thurtell, G. W., den Hartog, G., Neumann, H. H., and Staebler, R. M. (1997), Micrometeorological measurements of methane and nitrous oxide exchange above a boreal aspen forest, *J. Geophys. Res.* , 102(D24), 29331– 29341, doi:10.1029/97JD03181.
- Schiller, C. L., and Hastie, D. R. (1996), Nitrous oxide and methane fluxes from perturbed and unperturbed boreal forest sites in northern Ontario, *J. Geophys. Res.* , 101(D17), 22767– 22774, doi:10.1029/96JD01620.
- Speetjens, N.J., Hugelius, G., Gumbrecht, T., Lantuit, H., Berghuijs, W.R., Pika, P.A., Poste, A. and Vonk, J.E., 2023. The pan-Arctic catchment database (ARCADE). *Earth System Science Data* , 15 (2), pp.541-554.
- Stanley, E.H., Casson, N.J., Christel, S.T., Crawford, J.T., Loken, L.C. and Oliver, S.K., 2016. The ecology of methane in streams and rivers: patterns, controls, and global significance. *Ecological Monographs*, 86(2), pp.146-171.
- Terhaar, J., Lauerwald, R., Regnier, P. et al. Around one third of current Arctic Ocean primary production sustained by rivers and coastal erosion. *Nat Commun* 12, 169 (2021). <https://doi.org/10.1038/s41467-020-20470-z>
- Thornton, B. F., M. Wik, and P. M. Crill (2016), Double-counting challenges the accuracy of high-latitude methane inventories, *Geophys. Res. Lett.*, 43, 12,569–12,577, doi:10.1002/ 2016GL071772.
- Treat, CC, Bloom, AA, Marushchak, ME. Nongrowing season methane emissions –a significant component of annual emissions across northern ecosystems. *Glob Change Biol.* 2018; 24: 3331– 3343. <https://doi.org/10.1111/gcb.14137>
- Treharne, R., Rogers, B. M., Gasser, T., MacDonald, E., & Natali, S. (2022). Identifying Barriers to Estimating Carbon Release From Interacting Feedbacks in a Warming Arctic. *Frontiers in Climate*, 3. <https://doi.org/10.3389/fclim.2021.716464>
- Turetsky, M.R., Abbott, B.W., Jones, M.C. et al. Carbon release through abrupt permafrost thaw. *Nat. Geosci.* 13, 138–143 (2020). <https://doi.org/10.1038/s41561-019-0526-0>
- Ueyama, M., Iwata, H., Nagano, H., Tahara, N., Iwama, C. and Harazono, Y., 2019. Carbon dioxide balance in early-successional forests after forest fires in interior Alaska. *Agricultural and Forest Meteorology*, 275, pp.196-207.
- Ullah, S., Frasier, R., Pelletier, L. and Moore, T.R., 2009. Greenhouse gas fluxes from boreal forest soils during the snow-free period in Quebec, Canada. *Canadian Journal of Forest Research* ,39 (3), pp.666-680.
- van der Werf, G. R., Randerson, J. T., Giglio, L., van Leeuwen, T. T., Chen, Y., Rogers, B. M., Mu, M., van Marle, M. J. E., Morton, D. C., Collatz, G. J., Yokelson, R. J., and Kasibhatla, P. S.: Global fire emissions estimates during 1997–2016, *Earth Syst. Sci. Data*, 9, 697–720, <https://doi.org/10.5194/essd-9-697-2017>, 2017.
- Veraverbeke, S., Delcourt, C.J., Kukavskaya, E., Mack, M., Walker, X., Hessilt, T., Rogers, B. and Scholten, R.C., 2021. Direct and longer-term carbon emissions from arctic-boreal fires: A short review of recent advances. *Current Opinion in Environmental Science & Health*, 23, p.100277.

Virkkala, A.-M., Virtanen, T., Lehtonen, A., Rinne, J., & Luoto, M. (2018). The current state of CO₂ flux chamber studies in the Arctic tundra: A review. *Progress in Physical Geography: Earth and Environment*, 42 (2), 162–184. <https://doi.org/10.1177/0309133317745784>

Virkkala, A.-M., Natali, S. M., Rogers, B. M., Watts, J. D., Savage, K., Connon, S. J., Mauritz, M., Schuur, E. A. G., Peter, D., Minions, C., Nojeim, J., Commane, R., Emmerton, C. A., Goeckede, M., Helbig, M., Holl, D., Iwata, H., Kobayashi, H., Kolari, P., Lopez-Blanco, E., Marushchak, M. E., Mastepanov, M., Merbold, L., Parmentier, F.-J. W., Peichl, M., Sachs, T., Sonnentag, O., Ueyama, M., Voigt, C., Aurela, M., Boike, J., Celis, G., Chae, N., Christensen, T. R., Bret-Harte, M. S., Dengel, S., Dolman, H., Edgar, C. W., Elberling, B., Euskirchen, E., Grelle, A., Hatakka, J., Humphreys, E., Jarveoja, J., Kotani, A., Kutzbach, L., Laurila, T., Lohila, A., Mammarella, I., Matsuura, Y., Meyer, G., Nilsson, M. B., Oberbauer, S. F., Park, S.-J., Petrov, R., Prokushkin, A. S., Schulze, C., St. Louis, V. L., Tuittila, E.-S., Tuovinen, J.-P., Quinton, W., Varlagin, A., Zona, D., and Zyrjanov, V. I.: The ABCflux database: Arctic–boreal CO₂ flux observations and ancillary information aggregated to monthly time steps across terrestrial ecosystems, *Earth Syst. Sci. Data*, 14, 179–208, <https://doi.org/10.5194/essd-14-179-2022>, 2022.

Virkkala, A.-M., Aalto, J., Rogers, B. M., Tagesson, T., Treat, C. C., Natali, S. M., Watts, J. D., Potter, S., Lehtonen, A., Mauritz, M., Schuur, E. A. G., Kochendorfer, J., Zona, D., Oechel, W., Kobayashi, H., Humphreys, E., Goeckede, M., Iwata, H., Lafleur, P. M., Euskirchen, E. S., Bokhorst, S., Marushchak, M., Martikainen, P. J., Elberling, B., Voigt, C., Biasi, C., Sonnentag, O., Parmentier, F.-J. W., Ueyama, M., Celis, G., St. Louis, V. L., Emmerton, C. A., Peichl, M., Chi, J., Jarveoja, J., Nilsson, M. B., Oberbauer, S. F., Torn, M. S., Park, S.-J., Dolman, H., Mammarella, I., Chae, N., Poyatos, R., Lopez-Blanco, E., Christensen, T. R., Kwon, M. J., Sachs, T., Holl, D., and Luoto, M.: Statistical upscaling of ecosystem CO₂ fluxes across the terrestrial tundra and boreal domain: Regional patterns and uncertainties, *Global Change Biology*, 27, 4040–4059, <https://doi.org/10.1111/gcb.15659>, 2021.

Voigt, C., Marushchak, M.E., Lamprecht, R.E., Jackowicz-Korczyński, M., Lindgren, A., Mastepanov, M., Granlund, L., Christensen, T.R., Tahvanainen, T., Martikainen, P.J. and Biasi, C., 2017. Increased nitrous oxide emissions from Arctic peatlands after permafrost thaw. *Proceedings of the National Academy of Sciences*, 114 (24), pp.6238-6243.

Voigt, C., Marushchak, M.E., Abbott, B.W., Biasi, C., Elberling, B., Siciliano, S.D., Sonnentag, O., Stewart, K.J., Yang, Y. and Martikainen, P.J., 2020. Nitrous oxide emissions from permafrost-affected soils. *Nature Reviews Earth & Environment*, 1(8), pp.420-434.

Walker XJ, Mack MC, Johnstone JF. Stable carbon isotope analysis reveals widespread drought stress in boreal black spruce forests. *Glob Chang Biol*. 2015;21(8):3102-3113.

Walker, X.J., Baltzer, J.L., Cumming, S.G., Day, N.J., Ebert, C., Goetz, S., Johnstone, J.F., Potter, S., Rogers, B.M., Schuur, E.A. and Turetsky, M.R., 2019. Increasing wildfires threaten historic carbon sink of boreal forest soils. *Nature*, 572(7770), pp.520-523.

Walter Anthony, K.M., Anthony, P., Grosse, G. and Chanton, J., 2012. Geologic methane seeps along boundaries of Arctic permafrost thaw and melting glaciers. *Nature Geoscience*, 5(6), pp.419-426., DOI: 10.1038/ngeo1480

Walter Anthony, K., Schneider von Deimling, T., Nitze, I., Frohling, S., Emond, A., Daanen, R., Anthony, P., Lindgren, P., Jones, B. and Grosse, G., 2018. 21st-century modeled permafrost carbon emissions accelerated by abrupt thaw beneath lakes. *Nature communications*, 9(1), pp.1-11.

Watts, J. D., Farina, M., Kimball, J. S., Schiferl, L. D., Liu, Z., Arndt, K. A., Zona, D., Ballantyne, A., Euskirchen, E. S., Parmentier, F.-J., Helbig, M., Sonnentag, O., Tagesson, T., Rinne, J., Ikawa, H., Ueyama, M., Kobayashi, H., Sachs, T., Nadeau, D. F. . . . Oechel, W. C. (2023). Carbon uptake in Eurasian boreal forests dominates the high-latitude net ecosystem carbon budget. *Global Change Biology*, 29, 1870–1889. <https://doi.org/10.1111/gcb.16553>

Wik, M., Varner, R.K., Anthony, K.W., MacIntyre, S. and Bastviken, D., 2016. Climate-sensitive northern lakes and ponds are critical components of methane release. *Nature Geoscience*, 9(2), pp.99-105.

Wilkerson, J., Dobosy, R., Sayres, D.S., Healy, C., Dumas, E., Baker, B. and Anderson, J.G., 2019. Permafrost nitrous oxide emissions observed on a landscape scale using the airborne eddy-covariance method. *Atmospheric Chemistry and Physics*, 19 (7), pp.4257-4268.

Yang, G., Peng, Y., Marushchak, M.E., Chen, Y., Wang, G., Li, F., Zhang, D., Wang, J., Yu, J., Liu, L. and Qin, S., 2018. Magnitude and pathways of increased nitrous oxide emissions from uplands following permafrost thaw. *Environmental science & technology*, 52 (16), pp.9162-9169.

Yuan, Y., Zhuang, Q., Zhao, B., and Shurpali, N.: Nitrous oxide emissions from pan-Arctic terrestrial ecosystems: A process-based biogeochemistry model analysis from 1969 to 2019, EGUsphere [preprint], <https://doi.org/10.5194/egusphere-2023-1047>, 2023.

Supplementary material

Hosted file

RECCAP2_upscaling_A1.xlsx available at <https://authorea.com/users/659537/articles/663466-the-net-ghg-balance-and-budget-of-the-permafrost-region-2000-2020-from-ecosystem-flux-upscaling>

Hosted file

RECCAP2_upscaling_A2.xlsx available at <https://authorea.com/users/659537/articles/663466-the-net-ghg-balance-and-budget-of-the-permafrost-region-2000-2020-from-ecosystem-flux-upscaling>

Hosted file

RECCAP2_upscaling_A3.xlsx available at <https://authorea.com/users/659537/articles/663466-the-net-ghg-balance-and-budget-of-the-permafrost-region-2000-2020-from-ecosystem-flux-upscaling>

Hosted file

RECCAP2_upscaling_A4.xlsx available at <https://authorea.com/users/659537/articles/663466-the-net-ghg-balance-and-budget-of-the-permafrost-region-2000-2020-from-ecosystem-flux-upscaling>

Hosted file

RECCAP2_upscaling_A6.xlsx available at <https://authorea.com/users/659537/articles/663466-the-net-ghg-balance-and-budget-of-the-permafrost-region-2000-2020-from-ecosystem-flux-upscaling>

Hosted file

RECCAP2_upscaling_A5.xlsx available at <https://authorea.com/users/659537/articles/663466-the-net-ghg-balance-and-budget-of-the-permafrost-region-2000-2020-from-ecosystem-flux-upscaling>